THE IMPACT OF LONGWAVE RADIATIVE COOLING ON THE HEATING, MOISTURE AND WATER BUDGETS IN A TROPICAL AND A MIDLATITUDE SQUALL LINE

Wei-Kuo Tao and Joanne Simpson
Severe Storm Branch (Code 912)
Laboratory for Atmospheres
NASA/Goddard Space Flight Center
Greenbelt, MD 20771
U.S.A.

A two-dimensional, time-dependent and non-hydrostatic numerical cloud model is used to estimate the heating (Q_1), moisture (Q_2) and water budgets in the convective and stratiform regions for a tropical and a midlatitude squall line (EMEX and PRE-STORM). The model includes a parameterized three-class ice-phase microphysical scheme and longwave radiative transfer processes. A quantitative estimate of the impact of the longwave radiative cooling on the total surface precipitation as well as on the development and structure of these two squall lines will be made.

Longwave radiative cooling enhanced the total surface precipitation about 14% and 31% over a 16 h simulation time for the PRE-STORM and EMEX cases, respectively. A more significant effect is seen in the EMEX squall system due to the comparatively earlier development of the stratiform cloud. The effect of radiative cooling is shown to increase as systems age. The model results indicate that the Q_1 and Q_2 budgets in the convective and stratiform regions are only quantitatively, not qualitatively, altered by the inclusion or absence of the radiative transfer processes. Also, the radiative cooling does not change the overall squall structure (*i.e.*, propagation speed and multicellar characteristics) of these two squall systems. A ratio of the horizontal transfer of condensate from the convective line into the stratiform region to the amount of stratiform rain was reduced 10% to 23% by the inclusion of longwave radiative cooling in PRE-STORM and EMEX squall cases, respectively. This implies that a significant amount of condensate above the melting layer in the stratiform region of the EMEX case is generated by the longwave radiative processes.

1. INTRODUCTION

In a study of precipitation statistics of GATE Mesoscale Convective Systems (MCS), Houze (1977) estimated that four MCSs accounted for 50% of the rainfall at one of the GATE ships during Phase III. It was also estimated that the widespread stratiform rain accounted for about 29%-49% of the total rainfall for the GATE, WMONEX and midlatitudes MCSs These observational results clearly indicate the important contribution of stratiform precipitation. The distribution of heating in the stratiform region of MCSs is considerably different from the vertical profile of heating in the convective region (Houze, 1982; Johnson, 1984). Recently, many studies (Simpson *et al.*, 1988; Adler and Negri, 1988; Tao *et al.*, 1990) have also indicated that a separation of convective and stratiform clouds is necessary for a successful surface rain retrieval from remote sensors as well as a derivation of latent heating from various hydrometeor profiles.

An important question that has been studied in the past decade is: *what are the origins and growth mechanisms of particles in stratiform precipitation?* For example, Chen and Zipser (1982) suggested that both depositional growth associated with upward motion in the anvil and the horizontal flux of hydrometeors from the convective region are important in the maintenance of anvil precipitation. Gamache and Houze (1983) showed quantitatively that 25%-40% of the condensate which comprises the stratiform cloud was created by mesoscale ascent at mid-to-upper levels in the stratiform region of a GATE squall line. Gallus and Johnson (1991) found that the contribution to surface rainfall from condensation in the mesoscale updraft was comparable in magnitude to the transport of condensate rearward from the convective line at a rapidly weakening stage of a midlatitude squall line. Using a kinematic (steady-state) cloud model, Rutledge (1986) suggested that the condensate produced by mesoscale ascent is largely responsible for the large horizontal extent of light stratiform precipitation to the rear of the same case analyzed by Gamache and Houze (1983). Using higher resolution, Doppler-derived air motions associated with a midlatitude squall line as input in their two-dimensional kinematic model, Rutledge and Houze (1987) found that deposition in the mesoscale updraft accounted for 80% of the stratiform precipitation. They also conducted a series of sensitivity tests and found that almost no rain reached the surface in the stratiform region without the influx of hydrometeors from the convective cells, while only about one-fourth as much stratiform rain reached the surface in the absence of mesoscale ascent.

Recent numerical studies (Chen and Cotton, 1988; Dudhia, 1989; Tao *et al.*, 1991) clearly indicated that the circulation in the stratiform region, as well as the amount of total surface precipitation, can be enhanced by longwave radiative transfer processes. Yet, no details on the interaction between convective and stratiform regions (such as the transport of condensate rearward from the convective cells), as well as quantitative estimates of the effects of radiative cooling upon the amount of stratiform precipitation have been discussed in all these modeling studies. The major objective of this study is to calculate the heating (Q_1), moisture (Q_2) and water budgets in the convective and stratiform regions for an oceanic (EMEX) and a continental (PRE-STORM) squall line using a numerical model. The heating, moisture and water budgets will also be studied at various stages in the life cycles of the simulated squall systems.

2. THE MODEL

The tool used in this study is the two-dimensional (2-D) version of the Goddard Cumulus Ensemble (GCE) model (Tao and Soong, 1986; Tao and Simpson, 1989; Tao *et al.*, 1991). The

equations that govern cloud-scale motion are anelastic. The cloud microphysics include a parameterized Kessler-type two-category liquid water scheme (cloud water and rain), and parameterized three-category ice-phase schemes (cloud ice, snow and hail/graupel). Shortwave (solar) and longwave (infrared) radiation parameterizations are both included in the cloud model. Details of the model description can be found in Tao *et al.* (1991).

A stretched vertical coordinate (height increments from 220 to 1050 m) with 31 grid points is used in order to maximize resolution in the lowest levels of the model. The model top is about 20 km. The 2-D version of the model used 612 grid points in the horizontal, the central 504 of which comprised the fine grid area with a constant 750 m resolution. Simulated cloud activity was confined to the fine grid region through a Galilean transformation by subtracting the storm propagation speed from the initial wind field. Outside of this region, the grid was horizontally stretched with a ratio of 1.0625:1 between adjacent grid points. This resulted in a domain that was about 1025 km wide. Open-type lateral boundary conditions were used. The use of stretched horizontal coordinates causes the model results to be less sensitive to the choice of gravity wave speed associated with the open lateral boundary conditions (Fovell and Ogura, 1988). A 5-km deep Rayleigh relaxation (absorbing) layer is also used at the top of the model. A fourth-order horizontal advection scheme was used in the model with a time step of 7.5 s.

3. Q_1/Q_2 BUDGETS AND CONVECTIVE/STRATIFORM SEPARATION

In diagnostic studies (*e.g.*, Yanai *et al.*, 1973), it is customary to define the apparent heat source Q_1 and the apparent moisture sink Q_2 of a large-scale system by averaging horizontally the thermodynamic and water vapor equations as:

$$Q_1 = \bar{\pi}\left[\frac{\partial \bar{\theta}}{\partial t} + \bar{\vec{V}} \bullet \nabla \bar{\theta} + \bar{w}\frac{\partial \bar{\theta}}{\partial z}\right], \tag{1}$$

$$Q_2 = -\frac{L_v}{C_P}\left[\frac{\partial \bar{q}_V}{\partial t} + \bar{\vec{V}} \bullet \nabla \bar{q}_V + \bar{w}\frac{\partial \bar{q}_V}{\partial z}\right] \tag{2}$$

Q_1 and Q_2 can directly relate to the contributions of cloud effects which can be explicitly estimated by the GCE model (see Tao and Soong, 1986; Tao and Simpson, 1989):

$$Q_1 = \bar{\pi}[-\frac{1}{\bar{\rho}}\frac{\partial \bar{\rho}\overline{w'\theta'}}{\partial z} + D_\theta] + \frac{L_v}{C_P}(\bar{c} - \bar{e}_c - \bar{e}_r) + \frac{L_f}{C_P}(\bar{f} - \bar{m}) + \frac{L_s}{C_P}(\bar{d} - \bar{s}) + \bar{Q}_R \quad (3)$$

$$Q_2 = \frac{L_v}{C_P}[\frac{1}{\bar{\rho}}\frac{\partial \bar{\rho}\overline{w'q_V'}}{\partial z} - \bar{D}_{q_V}] + \frac{L_v}{C_P}(\bar{c} - \bar{e}_c - \bar{e}_r) + \frac{L_s}{C_P}(\bar{d} - \bar{s}) \quad (4)$$

The overbars denote horizontal averages, the primes indicate deviations from the horizontal averages. The variable $\bar{\rho}$ is the density and $\pi = (p / P_0)^{R/C_P}$ is the nondimensional pressure, where p is the dimensional pressure, P_O is the reference pressure taken to be 1000 mb, C_p is the specific heat of dry air at constant pressure and R is the gas constant for dry air. The variables L_V, L_f and L_S are the latent heats of condensation, fusion and sublimation, respectively. The variables c, e_c, e_r, f, m, d and s stand for the rates of condensation, evaporation of cloud droplets and raindrops, freezing of raindrops, melting of snow and graupel/hail, deposition of ice particles and sublimation of ice particles, respectively. The Q_R is the cooling/heating rate associated with radiative processes. Also the first terms on the right-hand side of (3) and (4) are the vertical eddy heat and moisture flux convergences, respectively. The subgrid scale turbulence terms are represented by D_θ and D_q.

The modeled squall system is first partitioned into convective and stratiform regions following techniques developed by Churchill and Houze (1984). Model grid points exhibiting *surface precipitation* and which have a rainfall rate twice as large as the averaged value taken over the four surrounding grid points are identified as convective cell cores. For each core grid point, the grid point residing on either side is also taken to be convective. Furthermore, any grid point with a rainrate in excess of 25 mm h^{-1} is designated as convective regardless of the above criteria. Precipitation at all other grid points is considered to be stratiform. However, because the Churchill and Houze separation technique is based on surface precipitation, two additional criteria have been added in order to classify those grid points having no surface precipitation (to be termed hereafter as "non-raining" region) as being either convective or stratiform in nature. A grid point with no surface precipitation is considered convective if cloud water is present (q_C > 0.1 g kg^{-1}) below the melting layer, or if the maximum updraft exceeds 5 m s^{-1}. Both criteria

are useful in identifying those regions where convection may be quite active aloft with little or no precipitation at the surface, such as areas associated with tilted updrafts and new cells initiated ahead of organized squall lines (Tao and Simpson, 1989). We also reclassify the grid points which were originally identified as stratiform but are located in front of the gust front as convective in order to give coherent areas of convective and stratiform rainfall. The Q_1 and Q_2 budgets which are derived from (3) and (4) will be separated into three distinctive regions, the convective, the stratiform and the trailing anvil without surface precipitation.

4. Water Budgets

In order to understand the interaction between convective and stratiform regions, it is necessary to estimate the horizontal transfer of hydrometeors between the two regions by calculating their water budgets (Gamache and Houze, 1983). Following a procedure first developed by Sui *et al.* (1991), the model results can be used to study the interaction between convective and stratiform regions quantitatively. The equations to predict cloud water(q_c), rain (q_r), cloud ice (q_i), snow(q_s) and graupel/hail (q_g) in the GCE model are:

$$\bar{\rho}\frac{\partial q_c}{\partial t} = -\frac{\partial}{\partial x}\bar{\rho}uq_c - \frac{\partial}{\partial z}\bar{\rho}wq_c + \rho(c - e_c) - T_{qc} \tag{5}$$

$$\bar{\rho}\frac{\partial q_r}{\partial t} = -\frac{\partial}{\partial x}\bar{\rho}uq_r - \frac{\partial}{\partial z}\bar{\rho}(w - V_r)q_r + \rho(c - e_r + m - f) - T_{qr} \tag{6}$$

$$\bar{\rho}\frac{\partial q_i}{\partial t} = -\frac{\partial}{\partial x}\bar{\rho}uq_i - \frac{\partial}{\partial z}\bar{\rho}wq_i + \rho(d_i - s_i) - T_{qi} \tag{7}$$

$$\bar{\rho}\frac{\partial q_s}{\partial t} = -\frac{\partial}{\partial x}\bar{\rho}uq_s - \frac{\partial}{\partial z}\bar{\rho}(w - V_s)q_s + \rho(d_s - s_s - m_s + f_s) - T_{qs} \tag{8}$$

$$\bar{\rho}\frac{\partial q_g}{\partial t} = -\frac{\partial}{\partial x}\bar{\rho}uq_g - \frac{\partial}{\partial z}\bar{\rho}(w - V_g)q_g + \rho(d_g - s_g - m_g + f_g) - T_{qg} \tag{9}$$

where V_r, V_s and V_g are the fall speeds of rain, snow and graupel, respectively, $m=m_s+m_g$, $f=f_s+f_g$. T_{qc}, T_{qr}, T_{qi},T_{qs} and T_{qg} are the transfer rates between hydrometeors and the sum of their values is zero. A more complete description associated with (5)-(9) can be found in Lin *et al.* (1983) and Rutledge and Hobbs (1984). By adding (5) through (9), the total hydrometeor equation becomes:

$$\bar{\rho}\frac{\partial q_t}{\partial t} = -\frac{\partial}{\partial x}\bar{\rho}uq_t - \frac{\partial}{\partial z}\bar{\rho}wq_t + \frac{\partial}{\partial z}\sum_i^3 \bar{\rho}V_i q_i + \rho(c-e+d-s) \qquad (10)$$

where $q_t=q_c+q_r+q_i+q_s+q_g$, $e=e_c+e_r$, $d=d_i+d_s+d_g$, $s=s_i+s_s+s_g$, and V_iq_i stands for V_rq_r, V_sq_s and V_gq_g. Vertical integration of (10) gives:

$$\int_{sfc}^{Z_T}\bar{\rho}\frac{\partial q_t}{\partial t}\Delta z = \int_{sfc}^{Z_T} -\frac{\partial}{\partial x}\bar{\rho}uq_t\Delta z - P_o + \int_{sfc}^{Z_T}\rho(c-e+d-s)\Delta z \qquad (11)$$

P_O is the surface precipitation rate in mm h^{-1}. Equation (11) can be further integrated horizontally over the convective, stratiform and non-raining regions, respectively, to give.

$$<\bar{\rho}\frac{\partial q_t}{\partial t}>_{Conv} = <-\frac{\partial}{\partial x}\bar{\rho}uq_t>_{Conv} - P_C + <\rho(c-e+d-s)>_{Conv} \qquad (12)$$

$$<\bar{\rho}\frac{\partial q_t}{\partial t}>_{Strf} = <-\frac{\partial}{\partial x}\bar{\rho}uq_t>_{Strf} - P_S + <\rho(c-e+d-s)>_{Strf} \qquad (13)$$

$$<\bar{\rho}\frac{\partial q_t}{\partial t}>_{Nsp} = <-\frac{\partial}{\partial x}\bar{\rho}uq_t>_{Nsp} + <\rho(c-e+d-s)>_{Nsp} \qquad (14)$$

where $<>=\int_x(\int_{sfc}^{Z_T}\Delta z)\Delta x$, P_C and P_S are the amounts of surface precipitation over the convective and stratiform regions, respectively. The first term on the right-hand-side of (12), (13) and (14) is the horizontal transfer term associated with the water budget. Our GCE model results can explicitly estimate each of the terms in (12), (13) and (14) over different time periods associated with various stages of the life cycle of the simulated squall systems.

5. LARGE-SCALE CONDITIONS AND MODEL INITIATION

A PRE-STORM event was chosen (June 10-11, 1985) for the midlatitude linear-type convective system simulation because it has good radar observations, and Q_1, Q_2 and water budget calculations are available (Rutledge *et al.*, 1988; Gallus and Johnson, 1991). A detailed description of this squall line's history and synoptic setting can be found in Johnson and Hamilton (1988). The squall line first developed ahead of a cold front and later grew to include a narrow but intense leading edge, a transition zone and a broad stratiform rain region. Several well-known features associated with midlatitude squall lines, such as a pre-squall mesolow, a squall mesohigh and a wake low, were also observed. The thermo-dynamic sounding from Pratt, Kansas was used as the initial condition (see Fig. 1a). Several different wind profiles associated with this squall line obtained from rawinsonde and profiler (Augustine and Zipser, 1987) data have been tested. These simulated results showed a small stratiform rain region and were not in good agreement with observations. The wind profile at upper levels in this PRE-STORM case was, then, modified [see Fig. 1c], and it resembles those used by Fovell and Ogura (1988) and Rotunno *et al* (1988).

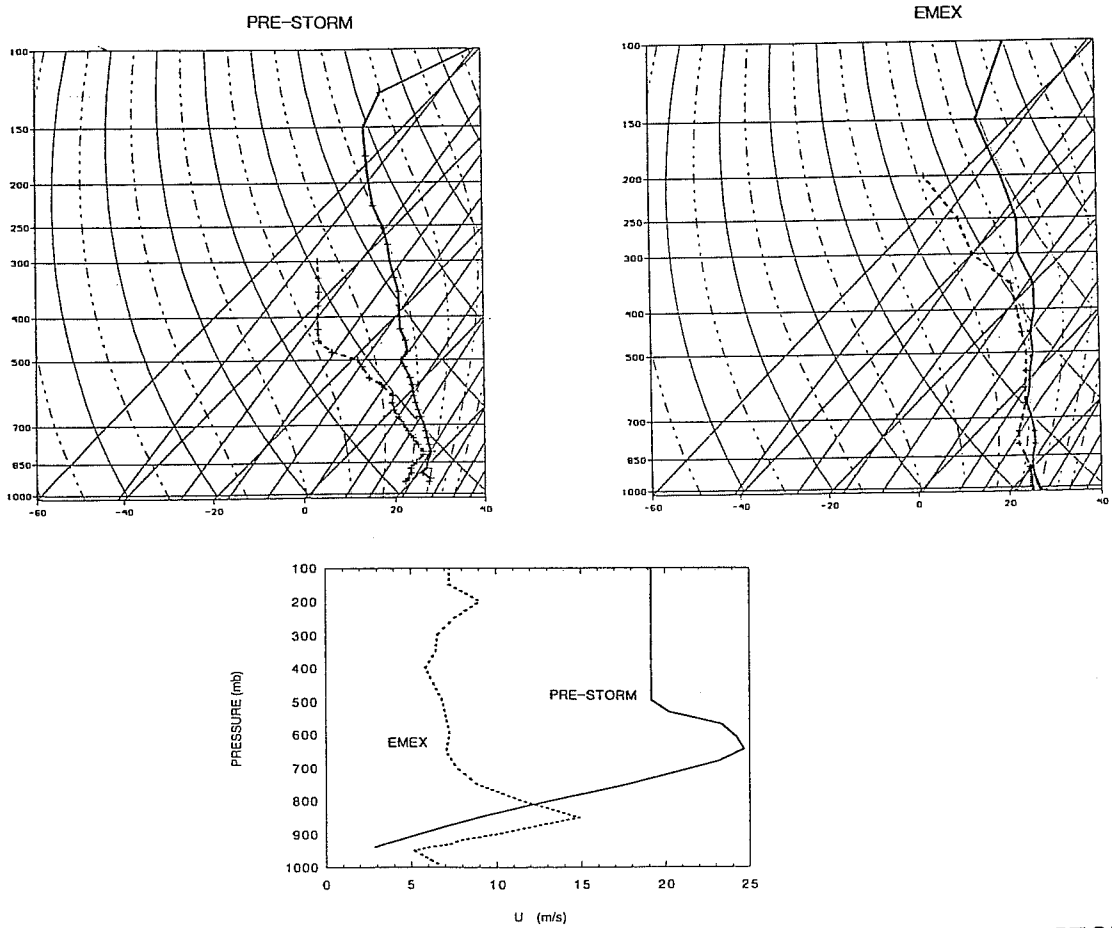

Fig. 1. Temperature and mixing ratio on a skew T-log p diagram for (a) PRE-STORM and (b) for EMEX case. (c) The normal components of wind used for the PRE-STORM and EMEX squall line simulation.

The EMEX9 precipitation system developed at the Arafura Sea (between Australia and New Guinea) and was under the influence of west-northwesterly monsoonal flow. The synoptic conditions as well as radar observations of this event have been described in detail by Webster and Houze (1991) and Bograd (1989). Radar observation first showed a single west-northwest to east-southeast oriented convective band (>300 km in length) embedded within a large region of stratiform precipitation. Later, two separate convective lines formed at the western end of the line. The western most system further developed into a squall line, and moved toward the northeast at 15-20 m s^{-1}. This squall line dominated over the second and was over 250 km in length with a large trailing stratiform rain region. Thermodynamic and wind profiles have been constructed by Alexander (1991) for use in cloud system simulations [Figs. 1b and 1c]. The data comprising these soundings below 400 mb in the environment ahead of the system are from the NOAA P-3 and NCAR Electra aircrafts. Above 400 mb the data are taken from objective synoptic analyses and interpolation between rawinsonde profiles.

The model initialization and microphysical schemes used in these two simulations are different, based on observational and previous modeling studies (see McCumber *et al.*, 1991). The graupel ice-phase microphysics have been selected for the EMEX simulations. On the other hand, hail rather than graupel has been included in the ice-phase microphysical processes for the PRE-STORM case. A weaker cool pool was used to initiate the convection in the EMEX case than in that of the PRE-STORM case (4.8 vs 6 ^{o}K over 10 minute period). In addition, surface fluxes of temperature and moisture using bulk aeordynamic formulas are included in the EMEX case. For each case, a pair of experiments (one including longwave radiative transfer processes and one without it) have been performed to assess the impact of longwave radiative cooling on the Q_1, Q_2 and water budgets.

6. RESULTS AND DISCUSSION

6.1 General cloud structure

Figure 2 shows the hydrometeor content (ice and water), pressure deviation and relative horizontal wind fields associated with the EMEX and PRE-STORM squall lines. The simulated PRE-STORM case captures qualitatively several important features discussed in Johnson and

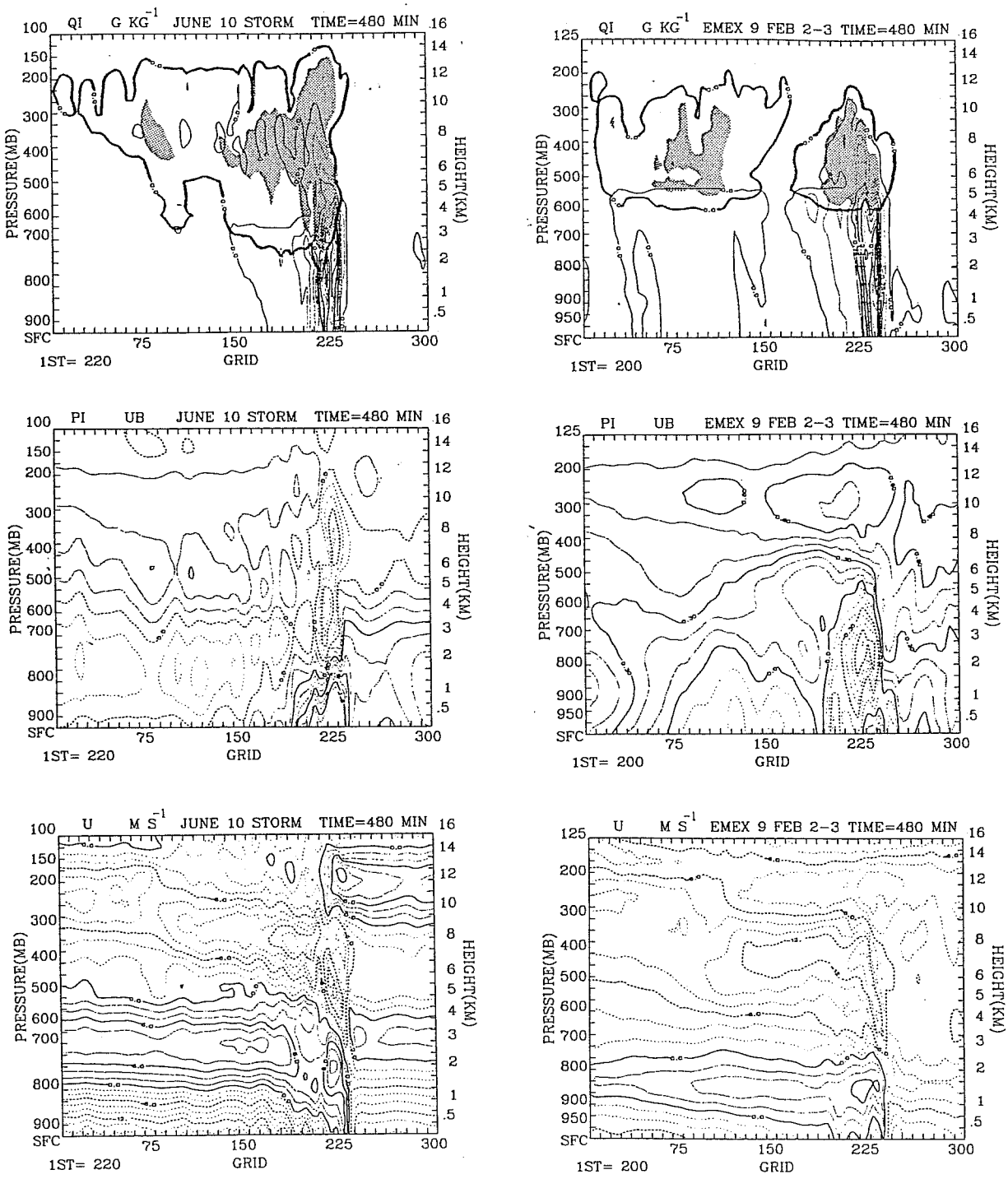

Fig. 2. Vertical cross section of ***(a)*** *the ice and water content,* ***(b)*** *the pressure deviation and* ***(c)*** *the wind speed relative to the squall line movement for the PRE-STORM case at its mature stage. The contour interval is .25 g kg^{-1}, 25 Pa and 2 m s^{-1} for (a), (b) and (c), respectively.* ***(d)***, ***(e)*** *and* ***(f)*** *same as* ***(a)***, ***(b)*** *and* ***(c)*** *except for the EMEX case.*

Hamilton (1988) and Rutledge *et al* (1988). For example, narrow convective cores are located at the leading edge of the system with a trailing wide-spread stratiform region. A squall meso-high and a wake low are well-simulated by the model for the PRE-STORM case. A 20-30 km wide transition zone which was observed during the mature and dissipating stages was not simulated by the model (see Fig. 3 in Rutledge *et al.*, 1988). In addition, a strong rear inflow that orginated at high altitude and some distance (200 to 300 km) from the leading edge of squall system was not simulated. A single sounding initiation for the non-hydrostatic model may restrict the model ability to capture these features. Nevertheless, the GCE model simulation did capture the observed rear inflow feature which was within 180 km of the leading edge (Figs. 6 and 7 in Rutledge *et al.*, 1988).

The EMEX case contained a wide stratiform region and it also produced a significant amount of startiform rain, typical of tropical oceanic MCS. The rear inflow as well as the squall meso-high and a wake low are also simulated by the model for the EMEX case. The rear inflow, however, is weaker and located in the low troposphere, compared with the PRE-STORM case. The maximum vertical velocity associated with the EMEX case is about 8 to 10 m s^{-1} and is comparable to that measured by the P-3 aircraft.

The model results also indicate that both EMEX and PRE-STORM systems move by discrete growth of new convective elements ahead of the old cells. New growth originates along the leading edge of the gust front, which is propelled by downdraft air from decaying convective cells. These features have been reported during several field experiments (*e.g.*, GATE, TAMEX, COPT-81 and PRE-STORM). These features have also been simulated by using non-hydrostatic cloud models (e.g., Rotunno *et al.*, 1988; Fovell and Ogura, 1988; Tao and Simpson, 1989; Lafore and Moncrieff, 1989; and many others). The lack of a decaying phase in simulated squall systems as reported by Fovell and Ogura (1988) is also evident for both cases. Two distinct differences between the two simulated cases have been found. The first noted difference is that new convection can develop 30 km ahead of an established updraft for the EMEX case. It is well-known that gravity waves can initialize new convection far away from the main convective event under preferred environmental conditions. The very moist environment of the EMEX case may provide this favorable condition. Another difference is that the time scale of new cell generation was about 15 and 30 minutes for PRE-STORM and EMEX cases, respectively. Previous model results (Dudhia *et al.*, 1987; and Fovell and Ogura; 1988) showed that new cell formation occurred every 30 min for the West Africa and Mid- Western squall cases. Balaji and Clark (1988) simulated cumulus cloud fields with surface fluxes superimposed with random temperature perturbations. They noted a 10-13 min time scale for

new cell generation for a midlatitude convective system, consistent with the observations. The time lapse between radar scans was too long to follow reliably individual updraft cell formation. The time scale of new cell generation has not been reported in both cases. A systematic modeling study in this respect will be needed.

The rainfall from the stratiform region for these two cases is shown in Table 1 using the convective-stratiform separation technique described in section 3. The EMEX case has more stratiform rain and its proportion of the total (42%) is in good agreement with MCSs observed during GATE and WMONEX. The stratiform rainfall for the PRE-STORM case is 10% less than estimated by Hamilton and Johnson (1988). The discrepancy between the modeled and observed stratiform rain amount may be caused by a simulation that is over a 16 h time period, which includes a developing stage. Figure 3 shows the hourly simulated rainfall information associated with the two squall cases. Only 7.5% of the rainfall from the total surface precipitation was categorized as stratiform for the first 4 h in the PRE-STORM case. Nevertheless, the PRE-STORM case exhibits a similar amount of stratiform rain analogues to that observed for an African tropical squall system over its whole lifetime (Chong, 1983). Another interesting feature is that stratiform rain developed rapidly for the EMEX simulation (Fig. 3). This feature is typical of the AMEX MCS (Frank and McBride, 1989).

TABLE 1

	Total-Rain (mm/grid/16h)	**Anvil Portion**	**$(\Delta P_c, \Delta P_s)$ (mm/grid/16h)**	**ΔP_o (%)**
EMEX9	**19.0**	**42%**	**(3.3,2.6)**	**31**
PreSTORM	**18.0**	**19%**	**(1.9,0.8)**	**14**

Table 1 Accumulated surface rainfall over the 16 h simulation time (in mm) normalized with respect to total model domain for PRE-STORM and EMEX squall lines. $(\Delta P_c, \Delta P_s)$ *are the difference of surface rainfall (in mm) between the experiments with and without longwave radiative cooling over the convective and stratiform regions, respectively.* ΔP_o *is the change (in percentage) in the total surface rainfall between the experiments with and without longwave radiative cooling.*

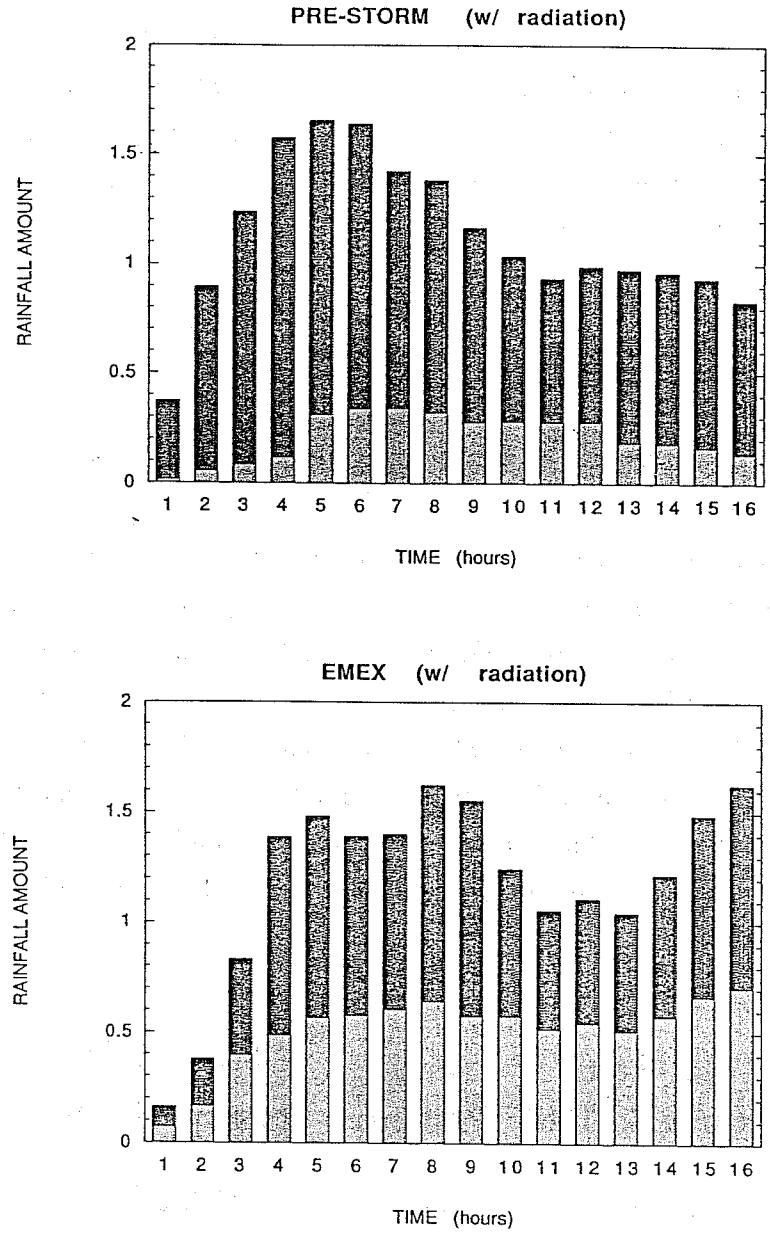

Fig. 3. Histogram plots of hourly accumulated rainfall for the (a) the PRE-STORM and (b) EMEX simulations. Lightly shaded regions are stratiform rain and darkly shaded portion represents the convective rainfall.

The GCE model results indicate that longwave radiative cooling enhanced the total surface precipitation about 14 and 31% over a 16 h simulation time in both cases, respectively (Table 1). Figure 4 shows the averaged radiative cooling rate over the clear, cloudy (convective + stratiform + non-raining), convective, stratiform and non-raining regions associated with the PRE-STORM and EMEX cases. The cooling of the cloud top and warming of the cloud base by the longwave radiation can destablize the stratiform cloud layer. These processes can have the

most impact on a well-developed stratiform cloud which usually occurs at the mature stage of the squall system. Also, note that both convective and stratiform precipitation increase when longwave radiative transfer processes are included (Table 1). This is because the clear air around the clouds cools more than the cloudy region due to longwave radiative cooling (see Fig. 4). The differential cooling between cloudy and clear regions can induce weak low-level convergence into the cloudy region and can enhance cloud activity as a whole. All these processes are functioning for both squall cases. A rapidly developing and deeper extent to the stratiform cloud layer was simulated for the tropical case. Thus, the radiative cooling had the largest effect for the EMEX case.

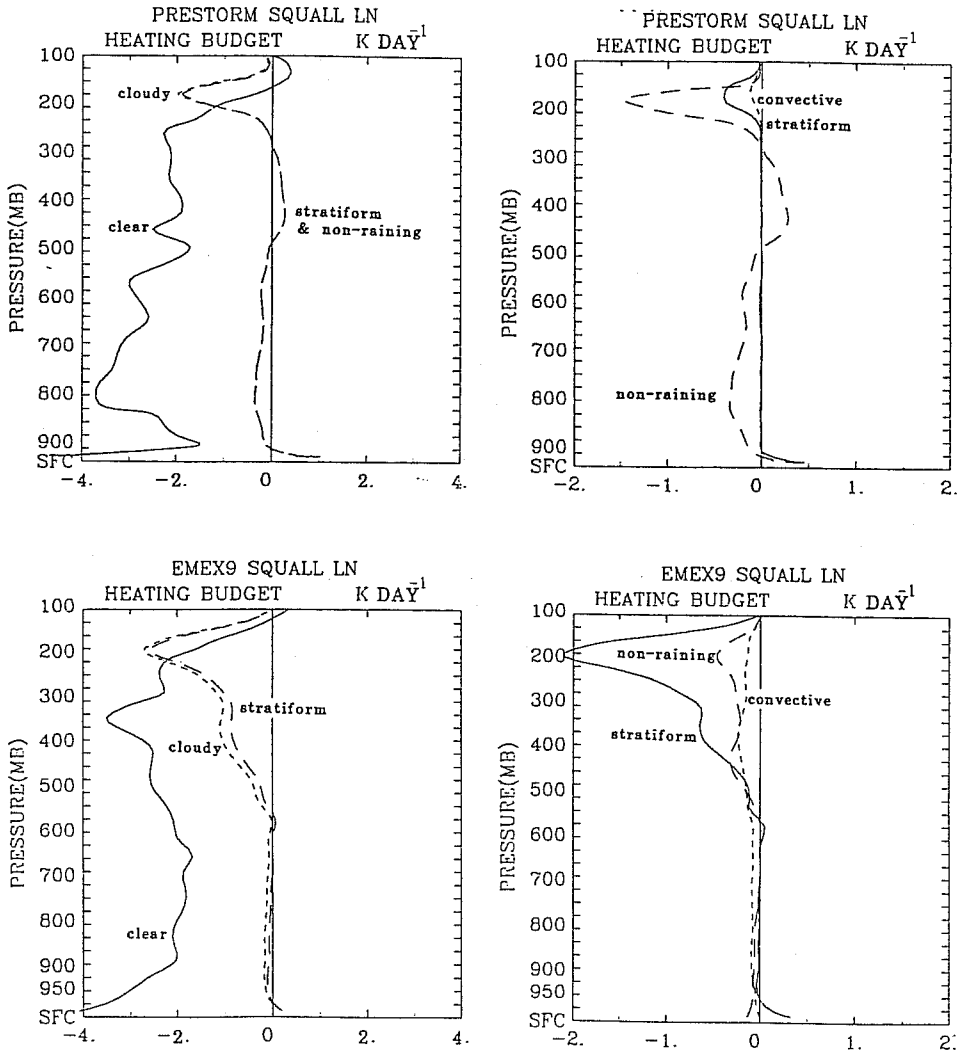

Fig. 4 (a) The averaged radiative cooling rate over the clear, cloudy and anvil (both stratiform and non-raining) region and (b) the radiative cooling over the convective, stratiform and non-raining regions for the PRE-STROM case. (c) and (d) same as (a) and (b) except for the EMEX case.

6.2 Q1 and Q2 budgets

Table 2 shows the individual components of the Q_1 and Q_2 budgets: condensation, evaporation, deposition, sublimation, melting, freezing, vertical eddy (heat and moisture) flux convergence and radiative cooling associated with these two different cases. These numbers were normalized with respect to their corresponding surface precipitation for comparison purposes. In the convective region, significant heating occurred due to the latent heat release by condensation in both cases. On the other hand, the condensation/deposition was almost balanced by evaporation/sublimation in the stratiform and the non-raining regions for the PRE-STORM case. A net heating in the stratiform region in the EMEX case is also a reflection of more stratiform rainfall generated in the EMEX case. The total amount of melted ice as well as frozen water hydrometeors is comparable to the amount of evaporated rain. The contribution of freezing/melting processes to the Q_1 budget is small, because the latent heat of fusion is an order of magnitude smaller than the latent heat of evaporation.

TABLE 2A
(PRE-STORM Squall Line)

	Total	Convective	Stratiform	Non-Raining
$\langle\bar{\rho}C\rangle$	1.47	1.13	0.27	0.07
$\langle\bar{\rho}E\rangle$	0.69	0.24	0.36	0.09
$\langle\bar{\rho}D\rangle$	0.74	0.22	0.33	0.19
$\langle\bar{\rho}S\rangle$	0.47	0.07	0.18	0.22
$\langle\bar{\rho}(C-E+D-S)\rangle$	1.05	1.04	0.06	-.05
$\langle\bar{\rho}m\rangle$	0.12	0.05	0.07	0.00
$\langle\bar{\rho}f\rangle$	0.09	0.06	0.03	0.00
$\langle\bar{\rho}w'T'\rangle^1$	0.29	0.24	0.18	0.07
$\langle\bar{\rho}w'q_v'\rangle^1$	0.95	0.92	0.78	0.17
$\langle\bar{\rho}Q_R\rangle$	-.23	-.00	-.00	-.05

TABLE 2B
(EMEX9 Squall Line)

	Total	Convective	Stratiform	Non-Raining
$<\bar{\rho}C>$	1.77	0.91	0.81	0.05
$<\bar{\rho}E>$	0.96	0.18	0.73	0.05
$<\bar{\rho}D>$	0.29	0.03	0.26	0.00
$<\bar{\rho}S>$	0.02	0.00	0.01	0.00
$<\bar{\rho}(C-E+D-S)>$	1.08	0.76	0.33	0.00
$<\bar{\rho}m>$	0.07	0.01	0.06	0.00
$<\bar{\rho}f>$	0.04	0.01	0.03	0.00
$<\bar{\rho}w'T'>^1$	0.16	0.08	0.11	0.01
$<\bar{\rho}w'q_v'>^1$	0.64	0.62	0.24	0.02
$<\bar{\rho}Q_R>$	-.28	-.01	-.05	-.02

$$< x >= \iint \rho x \Delta x \Delta z$$

[1]These fluxes are shown to be their absolute values.
All numbers are normalized to their corresponding surface rainfall rate (P_o)

Table 2 The individual components of the heating budget for (a) the PRE-STORM and (b) the EMEX squall lines. These numbers are averaged over a 16 h simulation time and are also normalized with respect to their surface rainfall. See text for more information.

The eddy vertical heat and moisture convergence will only redistribute the heat and moisture vertically as their vertically integrated values are zero. Thus, their absolute values are calculated in the Table 2. The vertical eddy moisture flux is a major contributor to the model-derived Q_2 budget for both cases. This result is consistent with our earlier work (Soong and Tao, 1980; Tao and Soong, 1986), and with COPT-81 studies (Lafore *et al.*, 1988; Chong and Hauser, 1990). In contrast, the contribution of eddy vertical heat convergence was only about 10% of that due to latent heat release by condensation for the EMEX case while nearly 20% for the PRE-STORM case. This resulted from a stronger vertical velocity associated with the PRE-STORM case. Another difference between these two cases is that the warm rain processes were dominant for the tropical oceanic squall case.

The individual components of the Q_1 and Q_2 budgets associated with these two different squall cases except for the experiments without longwave radiative transfer process have been calculated. It was found that the longwave radiative transfer processes only quanitatively change individual components of the Q_1 and Q_2 budgets. The longwave radiative transfer processes do not change the relative importance of each component in those budgets, nor do these processes change the overall simulated squall structures, such as propagation speeds and multicellular characteristics. A slightly bigger contribution from the eddy fluxes convergence terms in the Q_1 and Q_2 budgets was evident for the no-longwave cooling cases.

Large-scale models (General Circulation and Climate Models) require not only the global surface rainfall pattern but also the associated vertical distribution within the Q_1 and Q_2 budgets. The GCE model can help identify which processes should be parameterized by the large-scale model (*e.g.*, Table 2), as well as provide the information on vertical profiles of the Q_1 and Q_2 budget. Figure 5 shows Q_1 and Q_2 for the convective and stratiform regions for the EMEX and PRE-STORM squall cases. Examination of Fig. 5 suggests that there are many common features in the Q_1 profiles among the squall lines even though these systems occurred in very different geographic locations. For example, the convective heating is at a maximum in the lower and middle troposphere, whereas the stratiform (anvil) heating is maximized in the upper troposphere. Cooling is taking place in the stratiform region beneath the melting layer. These features are well-known for MCSs occurring in GATE, WMONEX, TAMEX, COPT-81 and PRE-STORM. The convective drying and stratiform moistening tend to offset each other in

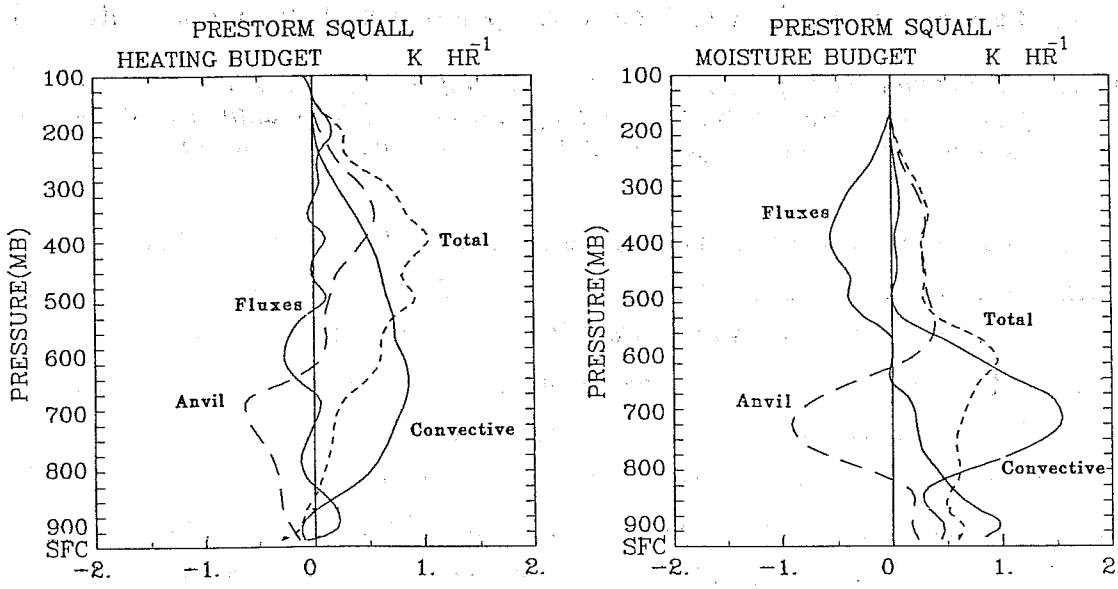

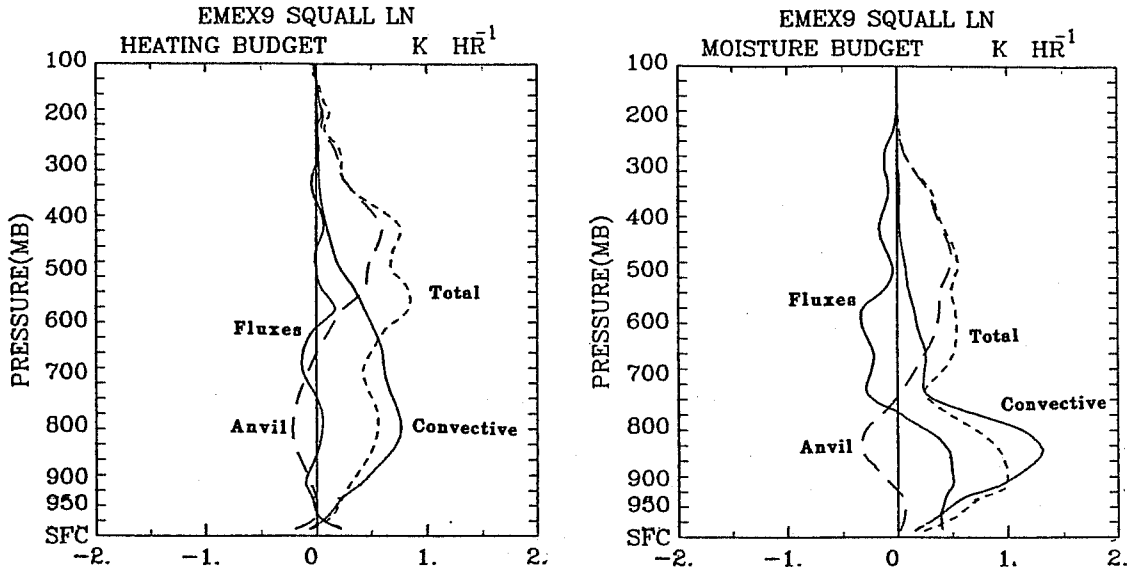

Fig. 5 (a) The heating and (b) the moisture budgets for the PRE-STORM squall line averaged over a 16 h simulation time. The contribution by its convective region, anvil (both stratiform and non-raining regions) region and the vertical eddy flux convergence components are also shown. The profiles of the convcetive and anvil regions also include their individual contribution of vertical eddy flux convergence term. (c)-(d) same as (a)-(b) except for the EMEX case.

the low levels in the Q_2 profiles for the PRE-STORM case. Low evaporative cooling in the EMEX case is indicative of high moisture content in the low to mid-troposphere. The mid-level minimum in the Q_2 profile for the EMEX case was due to vertical eddy transport in the convective region. The contribution to the total Q_1 budget by cloud-scale fluxes is minor for the EMEX case. The total vertical eddy heat flux is quite important in the low (below 900 mb) and mid-troposphere for the PRE-STORM. Also note that the importance of cloud-scale fluxes to the overall budget increases when the anvil and convective contributions nearly offset, as they do in the PRE-STORM case.

The Q_1 and Q_2 profiles for the convective and stratiform regions at the mature and initial stage (both averaged over a 4 h simulation time) were also computed by the modeled results for the EMEX and PRE-STORM squall cases. The mature stage of each simulated system is defined as the 4 h time period during which a maximum stratiform rain was developed (Fig. 3). The initial stage was simply obtained from the first 4 h simulation time. The Q_1 and Q_2 profiles at mature stage in these two cases showed a larger contribution by the stratiform region compared with those obtained during the initial stage. Strong heating in the upper troposphere for the Q_1 profile as well as a small contribution from the stratiform region to the Q_1 is evident for the PRE-STORM case. The Q_1 and Q_2 budgets at initial and mature stage for the EMEX

case are also quite similar to its corresponding 16 h averaged budgets (shown in Fig. 5) due to a rapid development of stratiform region. The vertical eddy moisture flux showed a greater contribution to the Q_2 budget at the initial stage in both cases. This is the main process to explain the different Q_2 profiles between the initial and mature stages of squall systems. For example, this process causes a stronger (moistening) mid-level minimum of Q_2 profile for the EMEX case. Also a stronger drying at low troposphere was found for the PRE-STROM case.

The GCE model simulated Q_1 budget is qualitatively in good agreement with that determined diagnostically from rawinsonde data for the PRE-STROM case (Fig. 9 in Gallus and Johnson, 1991). For example, several maxima in the Q_1 profile as well as cooling in the low troposphere estimated by Gallus and Johnson are captured by the simulation. The vertical eddy heat flux is partially responsible for the multi-peaks in the Q1 profiles for the PRE-STORM (Fig. 5). The total Q_2 profile is also in good agreement with that determined by Gallus and Johnson for the mature stage of the system. The simulated peak in the Q_1 profile contributed by the convective region is much lower than observed. This discrepancy may be due to the difference in area coverage attributed to the convective region between model and diagnostic studies. The modeled convective region is usually only 10 to 20 km in width and the average station spacing of the composited rawinsonde data was 80 km or more (see the discussion of Gallus and Johnson, 1990). The broad peak in heating between 550 and 400 mb as seen in the Q_1 profile for the simulated EMEX case is characteristic of tropical regions, and similar to the diagnostic study of AMEX cloud clusters by Frank and McBride (1989). Also a broad region of drying at lower and upper troposphere in the Q_2 budget for the mature to late stages of AMEX cloud clusters estimated by Frank and McBride is seen in the Q_2 results for the simulated EMEX case.

6.3 Water budgets

The water budgets in the convective, stratiform and non-raining regions associated with these two squall systems are shown in Figure 6. The water budgets are separated into three different layers: lower (surface to 10 ^{o}K level), middle (from 10 ^{o}K to -10 ^{o}K) and upper (-10 ^{o}K to 100 mb). The horizontal transfer of hydrometeors from the convective to the stratiform regions occurs mainly in the middle troposphere for the EMEX case. By contrast, two thirds of the horizontal transfer of hydrometeors is accomplished in the upper troposphere for the PRE-STORM case. Also a more vigorous transfer of hydrometeors in the lower troposphere from the stratiform region back into the convective region occurs for the PRE-STORM case. This is a consequence of the strong rear inflow simulated for this midlatitude case. A downward transfer

of hydrometeors from the middle to the lower troposphere is a dominant process in the stratiform regions for both two cases. The interaction between the stratiform and non-raining region is less significant than that between the convective and stratiform region.

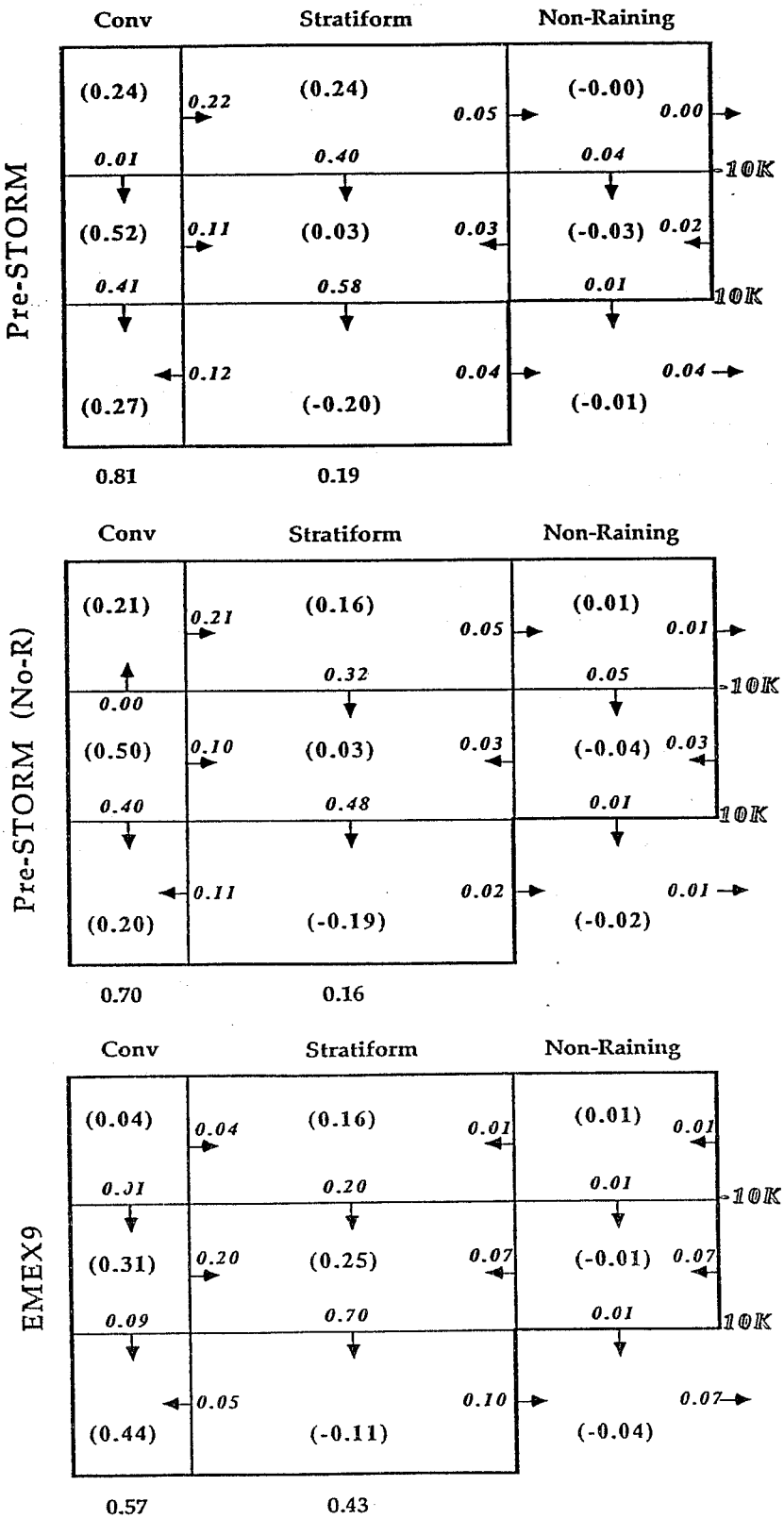

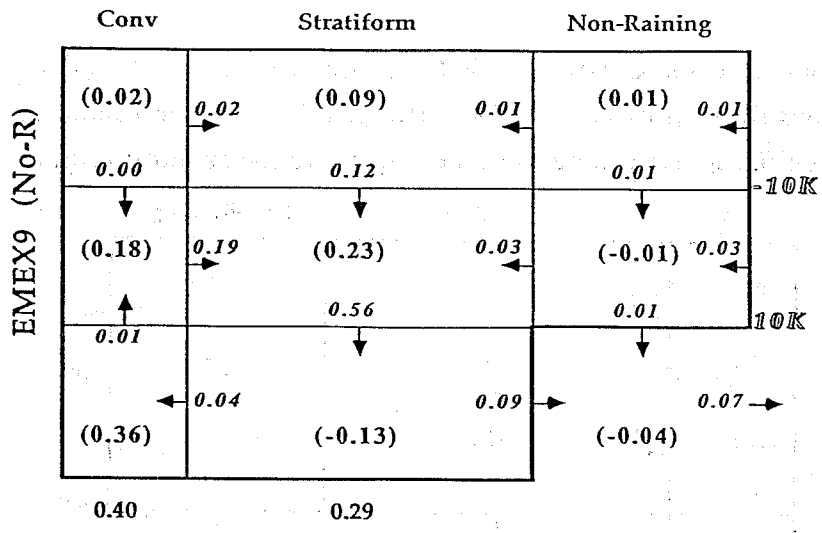

Fig. 6. The water budgets for (a) PRE-STORM and (c) EMEX simulated squall systems. Italic numbers indicate the amount of condensate transfer between various regions and layers while quantities in parenthese are the net condensation generated through microphysical processes. (b) and (d) same as (a) and (c) except for the experiment without longwave radiative transfer processes.

The contribution to stratiform rain by the convective region can be estimated quantitatively by the ratio shown in Table 4. A small ratio indicates a small contribution to the stratiform rain by horizontal transfer processes from the convective region. The ratio associated with the PRE-STORM case over the 16 h simulation is 1.74. This implies an important role for the convective region in the generation of stratiform rainfall. By contrast, the EMEX case has more stratiform rainfall than its PRE-STORM counterpart, and interestingly, the ratio is only 0.56. Another important finding is that both cases exhibited less horizontal transport of hydrometeors from the convective region into the stratiform region during their mature stages.

The longwave radiative transfer processes can increase net condensation at upper layers in the convective, stratiform and non-raining regions (Fig. 6). Consequently, they can have an important impact on the degree of horizontal transfer of hydrometeors into the stratiform region for these two cases. Both the EMEX and PRE-STORM cases show a decrease in this ratio when longwave radiative transfer processes are included (Table 3). The ratio was reduced by 23% with the inclusion of longwave radiative transfer processes in the EMEX case. A smaller reduction in this ratio (10%) was estimated for the PRE-STORM case. This implies that the longwave radiative cooling can be responsible for a significant generation of hydrometeors (through condensation/deposition) in the upper troposphere which ultimately, descend to form stratiform rain in the tropical case.

TABLE 3

	Radiation (16 h)	I-Stage (4h)	M-Stage (4h)	No-Rad (16h)
EMEX9	0.56	0.85	0.42	0.72
PreSTORM	1.74	562.	0.93	1.94

Table 3 The ratio of horizontal transfer of condensate from the convective to stratiform region above the 10 ^{o}K level to the amount of surface rainfall in the stratiform region for the entire 16 h period, both with and without longwave radiative cooling. The 4 h period corresponding to the initial and mature stages is also shown.

The ratio of the condensate carried from the convective line into the stratiform region to surface rainfall in the stratiform region for five different GATE MCSs and one midlatitude squall line is shown in Table 4. These values are derived from the observed-composite thermodynamic and wind fields associated with MCS (see Leary and Houze, 1980; Gamache and Houze, 1983; and Gallus and Johnson, 1991). Five out of six observed cases showed that the ratio is very close to unity. This implies that the convective region plays a very important role in the generation of stratiform rain. The modeled EMEX case indicates a relatively small contribution (56%) of the horizontal condensate is transfered from the convective region to the stratiform precipitation at the surface. The ratio at the initial stage of the simulated EMEX case is closer to the five MCSs shown in Table 5. Also, a good agreement is evident between the ratio at the mature stage of the modeled PRE-STORM squall system and that estimated by Gallus and Johnson (1991). Nevertheless, a direct comparion between these studies and the current model study should be done with caution, because a different spatial resolution, and a different definition for the convective-stratiform region here used. The comparison between the simulated PRE-STORM and EMEX cases, however, is consistent because the same type of data set and the same criteria for partitioning the convective and stratiform regions were used.

TABLE 4

CASE	Anvil Portion	Ratio (%)
LH-A	0.40	1.10
LH-B	0.40	2.00
LH-C	0.40	1.00

GH-I	0.49	0.86
GH-2	0.49	1.04
GJ-June10	0.30	0.87

Table 4 The same ratio defined in Table 4 except for MCS cases, A, B and C of Leary and Houze (1980), cases I and II of Gamache and Houze (1983) and the 10-11 June squall line of Gallus and Johnson (1991).

7. SUMMARY AND CONCLUSIONS

A two-dimensional, time-dependent and non-hydrostatic numerical cloud model has been used to estimate the heating (Q_1), moisture (Q_2) and water budgets in the convective and startiform regions for a tropical (EMEX) and a midlatitude (PRE-STORM) squall line. For each case, a pair of experiments (one including longwave radiative transfer processes and one without it) have been performed. A quantitative estimate of the impact of the longwave radiative cooling on the production of surface precipitation as well as the development and structure of these two squall lines, then, have been made. The environmental conditions associated with these two squall systems are quite different. For example, the corresponding CAPE (Convective Available Potential Energy) for the EMEX squall line is much smaller (1484 $m^2 s^{-2}$) than that of the PRE-STROM case (2300 $m^2 s^{-2}$). Also, the vertically integrated water vapor contents are 6.175 and 4.385 g g^{-1} cm^{-2} for EMEX and PRE-STROM cases, respectively. A very moist environment in the pacific region (WMONEX, AMEX) is quite common.

Overall, the simulated squall systems captured several important features which have been observed. For example, an intense leading edge and a broad stratiform rain region were simulated in both squall cases. Several well-known features associated with midlatitude squall lines, such as a squall mesohigh, a wake low, and a rear inflow, were also simulated in the two cases. These simulated features are much weaker in the tropical case than those associated with the midlatitude one. The model results also indicate that both EMEX and PRE-STORM systems move by discrete growth of new convective elements ahead of the old cells. New growth originates along the leading edge of the gust front, which is propelled by downdraft air from decaying convective cells. These features have been reported during several field experiments (*e.g.*, GATE, TAMEX, COPT-81 and PRE-STORM).

The GCE simulated Q_1 and Q_2 profiles at the mature stage of the PRE-STORM case are in a good agreement with those determined diagnostically using rawinsonde data (Gallus and Johnson, 1991). Overall, the Q_1 and Q_2 profiles for the simulated EMEX case are characteristic

of tropical regions, and similar to the diagnostic study of AMEX cloud clusters by Frank and McBride (1989). Low evaporative cooling in the EMEX case is indicative of high moisture content in the low to mid-troposphere. There are many common features in the Q_1 profiles among these two squall lines. For example, the convective heating is at a maximum in the lower and middle troposphere, whereas the stratiform (anvil) heating is maximized in the upper troposphere. Cooling is taking place in the stratiform region beneath the melting layer. These features are well-known for MCSs occurring in GATE, WMONEX, TAMEX and COPT-81. The heating and moisture budgets at various stages in the life cycles of the simulated squall systems were also calculated. The Q_1 and Q_2 budgets for the initial and mature stages of the EMEX case are also quite similar to its corresponding 16 h averaged budgets due to the rapid development of the stratiform region. By contrast, a small contribution by the stratiform region in Q_1 and Q_2 budgets was found in the PRE-STORM case during its initial stage.

The vertical eddy moisture flux is a major contributor to the model-derived Q_2 budget in both squall cases. This result is consistent with our earlier work (Soong and Tao, 1980; Tao and Soong, 1986), and with COPT-81 studies (Lafore *et al.*, 1988; Chong and Hauser, 1990). The distinct mid-level minimum in the Q_2 profile for the EMEX case is due to vertical eddy transport in the convective region. The contribution to the Q_1 budget by cloud-scale fluxes is minor for the EMEX case. This result is also consistent with our earlier work on GATE MCS simulations and with COPT-81 studies. By contrast, the vertical eddy heat flux is quite important in the low (below 900 mb) and mid-troposphere for the PRE-STORM case. This resulted from a stronger vertical velocity associated with the PRE-STORM case. This vertical eddy heat flux is also partially responsible for the multi-peaks in the Q_1 profiles for the PRE-STORM case.

Water budgets in the convective and stratiform region were calculated for both squall systems. The horizontal transfer of hydrometeors from the convective region to the stratiform region occurs mainly in the middle troposphere for the EMEX case. In contrast, two thirds of the horizontal transfer of hydrometeors is accomplished in the upper troposphere for the PRE-STORM case. The contribution of stratiform rain from the convective region can be estimated quantitatively by the ratio between the horizontal transfer of hydrometeors from the convective region above 10 ^{o}K to the amount of surface rainfall in the stratiform region. It was found that the convective region plays an important role in the generation of stratiform rainfall in the PRE-STORM case. The EMEX case has more stratiform rainfall than its PRE-STORM counterpart and the ratio is only about one third of that associated with the PRE-STORM case. Another finding is that both cases exhibited less horizontal transport of hydrometeors from the

convective region into the stratiform region during their mature stages than during their earlier stages.

Longwave radiative cooling enhanced the total surface precipitation by 14% and 31% over the 16 h simulation time for the PRE-STORM and EMEX cases, respectively. A more significant effect on the EMEX squall system is caused by the earlier development of the stratiform cloud. A ratio of the horizontal transfer of condensate from the convective line to the stratiform region, to the amount of stratiform rain was reduced to 10% to 23% by the inclusion of longwave radiative cooling in these two squall cases. This implies that a significant amount of condensate above the melting layer in the stratiform region of the EMEX case is generated by longwave radiative processes. The model results also indicate that Q_1 and Q_2 budgets in the convective and stratiform regions are only quantitatively, not qualitatively, altered by the inclusion or absence of radiative transfer processes. Also, the radiative cooling does not change the overall squall structure, such as propagation speed and multicellar characteristics of these two squall systems.

This study is a first step in an effort to quantitatively estimate how cloud and longwave radiative transfer processes interact with each other. Solar radiation plays an important role in the cloud-radiation interaction (*e.g.*, Tripoli and Cotton, 1989), and its effect on the formation of various types of cloud systems needs to be studied. The sensible and latent heat fluxes from the ocean can also affect the water budgets as well as the organization of cloud systems in the Western Pacific (see Sui *et al.*, 1991). In addition, cloud microphysical processes, heat fluxes form the warm ocean and radiative transfer processes should interact with each other. How these processes act under different environmental conditions will be a main focus of modeling studies in the future.

8. ACKNOWLEDGEMENT

The authors thank Dr. Johnson for providing the PRE-STORM sounding and Dr. W. Frank for providing the AMEX heating and moisture budgets. The EMEX sounding was obtained through Dr. G. Young.

The work is supported by the NASA Headquarters Mesoscale Processes Program under Contract 460-23-54 and by NASA TRMM project under Contract 460-63-58. These authors are grateful to Drs. J. Theon and R. Kakar for their support of this research. Acknowledgment is also made to NASA/ Goddard Space Flight Center for computer time used in the research.

9. REFERENCES

Adler, R. F., and A. J. Negri, 1988: A satellite infrared technique to estimate tropical convective and stratiform rainfall. *J. Appl. Meteor.*, **27**, 30-51.

Alexander, G., D., 1991: The relationship between EMEX mesoscale precipitation feature properties and their environmental characteristics. M. S. Thesis, Department of Meteorology, The Pennsylvania State University, University Park, PA. XX pp.

Augustine, J. A., and E. J. Zipser, 1987: The use of wind profilers in a mesoscale experiment. *Bull. Amer. Meteor. Soc.*, **68**, 4-17.

Balaji, V, and T. L. Clark, 1988: Scale selection in locally forced convective fields and the initiation of deep clouds. *J. Atmos. Sci.*, **45**, 3188-3211.

Bograd, S. J., 1989: The mesoscale structure of precipitation in EMEX cloud clusters, M. S. Thesis, Department of Atmospheric Sciences, University of Washington, Seattle, WA, XX pp.

Chen, S., and W. R. Cotton, 1988: The sensitivity of a simulated extra-tropical mesoscale convective system to long-wave radiation and ice-phase microphysics. *J. Atmos. Sci.*, **45**, 3897-3910.

Chen, Y.-L., and E. J. Zipser, 1982: The role of horizontal advection of hydrometeors in the water budget of a large squall system. *Preprints, 12th Conf. on Severe Local Storms*, San Antonio, Amer. Meteor. Soc., 355-358.

Chong, M., 1983: Les radars meteorologiques Doppler pour l'etude de la convection orageuse: Application a l'etude d'une ligne de grains tropicale. These de Doctorat d'Etat, Universite de Paris VI, 140 pp.

Chong, M. and D. Hauser, 1990: A tropical squall line observed during the COPT 81 experiment in West Africa. Part III: Heat and moisture budgets. *Mon. Wea. Rev.*, **118**, 1696-1706.

Churchill, D. D., and R. A. Houze, Jr., 1984: Development and structure of winter monsoon cloud clusters on 10 December 1978. *J. Atmos. Sci.*, **41**, 933-960.

Dudhia, J., 1990: Numerical study of convection observed during the Winter Monsoon Experiment using a mesoscale two-dimensional model. *J. Atmos. Sci.*, **46**, 3077-3107.

Dudhia, J., M. W. Moncrieff and D. W. K. So, 1987: The two-dimensional dynamics of west African squall lines. *Quart. J. Roy. Meteor. Soc.*, **113**, 567-582.

Fovell, R. G., and Y. Ogura, 1988: Numerical simulation of a midlatitude squall line in two-dimensions. *J. Atmos. Sci.*, **45**, 3846-3879.

Frank, W. M., and J. L. M. Bride, 1989: The vertical distribution of heating in AMEX and GATE cloud clusters. *J. Atmos. Sci.*, **46**, 3464-3478.

Gallus, W. A., Jr. and R. H. Johnson, 1991: Heat and moisture budgets of an intense midlatitude squall line. *J. Atmos. Sci.*, **48**, xxxx-xxxx.

Gamache, J. F., and R. A. Houze, Jr., 1983: Water budget of a mesoscale convective system in the tropics. *J. Atmos. Sci.*, **40**, 1835-1850.

Houze, R. A., Jr., 1977: Structure and dynamics of a tropical squall-line system. *Mon. Wea. Rev.*, **105**, 1540-1567.

Houze, R. A., Jr., 1982: Cloud clusters and large-scale vertical motions in the tropics. *J. Meteor. Soc. Japan, 60*, 396-409.

Johnson, R. H., 1984: Partitioning tropical heat and moisture budgets into cumulus and mesoscale components: Implication for cumulus parameterization. *Mon. Wea. Rev.*, **112**, 1656-1665.

Johnson, R. H. and P. J. Hamilton, 1988: The relationship of surface pressures to the precipitation and airflow structure of an intense midlatitude squall line.*Mon. Wea. Rev.*, **116**, 1444-1471.

LaFore, J.-P. and Moncrieff, 1989: A numerical investigation of the origination and interaction of the convective and stratiform regions of tropical squall lines. *J. Atmos. Sci.*, **46**, 521-544.

Lafore, J.-P., J.-L. Redelsperger and G. Jaubert, 1988: Comparison between a three-dimensional simulation and Doppler radar data of a tropical squall line: Transport of mass, momentum, heat, and moisture. *J. Atmos. Sci.*, **45**, 3483- 3500.

Leary, C. A., and R. A. Houze, Jr., 1980: The contribution of mesocale motions to the mass and heat fluxes of an intense tropical convective system. *J. Atmos. Sci.*, **37**, 784-796.

Lin, Y.-L., R. D. Farley and H. D. Orville, 1983: Bulk parameterization of the snow field in a cloud model. *J. Clim. Appl. Meteor.*, **22**, 1065-1092.

McCumber, M., W.-K. Tao, J. Simpson, R. Penc, and S.-T. Soong, 1991: Comparison of ice-phase microphysical parameterization schemes using numerical simulations of convection. *J. Appl. Meteor.*, 30, 985-1004.

Rotunno, R., J. B. Klemp and M. L. Weisman, 1988: A theory for strong, long-lived squall lines. *J. Atmos. Sci.*, **45**, 463-485.

Rutledge, S. A., 1986: A diagnostic modeling study of the stratiform region associated with a tropical squall line. *J. Atmos. Sci.*, **43**, 1356-1377.

Rutledge, S.A., and P.V. Hobbs, 1984: The mesoscale and microscale structure and organization of clouds and precipitation in midlatitude clouds. Part XII: A diagnostic modeling study of precipitation develop-ment in narrow cold frontal bands. *J. Atmos. Sci.*, **41**, 2949-2972.

Rutledge, S. A., and R. A. Houze, Jr., 1987: A diagnostic modeling study of the trailing stratiform of a midlatitude squall line. *J. Atmos. Sci.*, **44**, 2640-2656.

Rutledge, S. A., R. A. Houze, Jr., M. I. Biggerstaff and T. Matejka, 1988: The Oklahoma-Kansas mesoscale convective system of 10-11 June 1985: Precipitation structure and single-Doppler radar analysis.*Mon. Wea. Rev.*, **116**, 1409-1430.

Simpson, J., R. F. Adler and G. R. North, 1988: A proposed satellite tropical rainfall measuring mission (TRMM). *Bull. Amer. Meteor. Soc.*, **69**, 278-295.

Soong, S.-T., and W.-K. Tao, 1980: Response of deep tropical clouds to mesoscale processes. *J. Atmos. Sci.*, **37**, 2035-2050.

Sui, C.-H., K.-M. Lau, W.-K. Tao and J. Simpson, 1991: A study of water budget in tropical convective systems: Application to climate change. *Fifth Conf. on Climate Variations*, Amer. Meteor. Soc., Denver, Colo.

Tao, W.-K., and J. Simpson, 1989: Modeling study of a tropical squall-type convective line. *J. Atmos. Sci.*, **46**, 177-202.

Tao, W.-K., and S.-T. Soong, 1986: A study of the response of deep tropical clouds to mesoscale processes: Three-dimensional numerical experiments. *J. Atmos. Sci.*, **43**, 2653-2676.

Tao, W.-K., J. Simpson, S. Lang, M. McCumber, R. Adler and R. Penc, 1990: An algorithm to estimate the heating budget from vertical hydrometeor profiles. *J. Appl., Meteor.*, **29**, 1232-1244.

Tao, W.-K., J. Simpson and S.-T. Soong, 1991 Numerical simulation of a sub-tropical squall line over Taiwan Strait. *Mon. Wea. Rev.*, **119**, (November issue).

Webster, P. J. and R. A. Houze, Jr., 1991: The Equatorial Mesoscale Experiment (EMEX): An overview, *Bull. Amer. Meteor. Soc.*, (in press).

Yanai, M., S. Esbensen and J. Chu, 1973: Determination of average bulk properties of tropical cloud clusters from large-scale heat and moisturebudgets *J. Atmos. Sci.*, **30**, 611-627.